LETTER **Communicated by Maxim Bazhenov**

Bifurcation Analysis of Jansen's Neural Mass Model

François Grimbert
Francois.Grimbert@sophia.inria.fr
Olivier Faugeras
Olivier.Faugeras@sophia.inria.fr
Odyssée Laboratory, INRIA/ENPC/ENS, INRIA Sophia-Antipolis, 06902 Sophia Antipolis, France.

We present a mathematical model of a neural mass developed by a number of people, including Lopes da Silva and Jansen. This model features three interacting populations of cortical neurons and is described by a six-dimensional nonlinear dynamical system. We address some aspects of its behavior through a bifurcation analysis with respect to the input parameter of the system. This leads to a compact description of the oscillatory behaviors observed in Jansen and Rit (1995) (alpha activity) and Wendling, Bellanger, Bartolomei, and Chauvel (2000) (spike-like epileptic activity). In the case of small or slow variation of the input, the model can even be described as a binary unit. Again using the bifurcation framework, we discuss the influence of other parameters of the system on the behavior of the neural mass model.

1 Introduction

Jansen's neural mass model is based on the work of Lopes da Silva, Hoeks, and Zetterberg (1974), Lopes da Silva, van Rotterdam, Barts, van Heusden, and Burr (1976), and van Rotterdam, Lopes da Silva, van den Ende, Viergever, and Hermans, (1982). They developed a biologically inspired mathematical framework to simulate spontaneous electrical activities of neurons assemblies recorded by EEG, with a particular interest for alpha activity. In their model, populations of neurons interact by excitation and inhibition and can, in effect, produce alpha activity. Jansen, Zouridakis, and Brandt (1993) and Jansen and Rit (1995), discovered that this model was also able to simulate evoked potentials, that is, EEG activities observed after a sensory stimulation (such as a flash of light or a sound). More recently, Wendling, Bellanger, Bartolomei, and Chauvel (2000) used this model to synthesize activities very similar to those observed in epileptic patients, and David and Friston (2003); David, Cosmelli, and Friston (2004) studied connectivity between cortical areas with a similar framework.

The contribution of this letter is a fairly detailed description of the behavior of this particular neural mass model as a function of its input. This

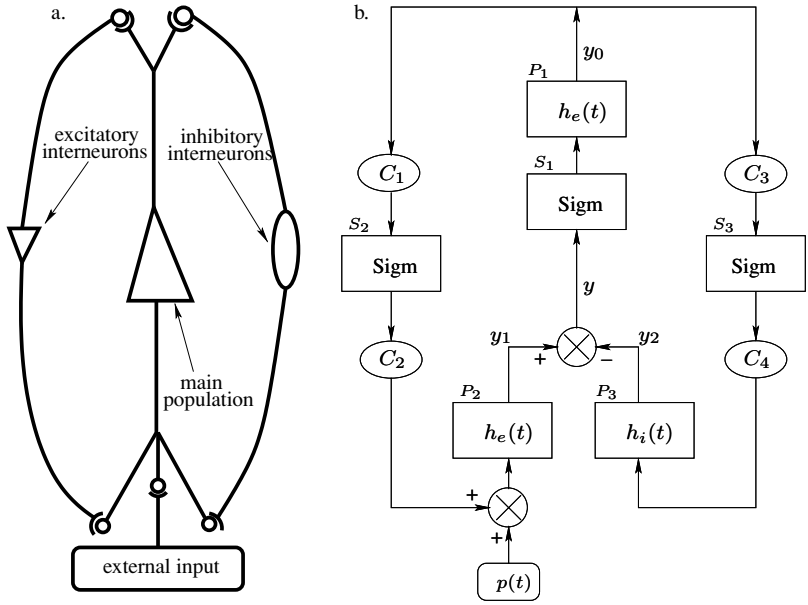

Figure 1: (a) Neural mass model of a cortical unit. It features a population of pyramidal cells interacting with two populations of interneurons—one excitatory (left branch) and the other inhibitory (right branch). (b) Block representation of a unit. The h boxes simulate synapses between the neuron's populations. Sigm boxes simulate cell bodies of neurons by transforming the membrane potential of a population into an output firing rate. The constants C_i model the strength of the synaptic connections between populations.

description is grounded in the mathematics of dynamic systems and bifurcation theories. We briefly recall the model in section 2 and describe in section 3 the properties of the associated dynamical system.

2 Description of the Model.

The model features a population of pyramidal neurons (see the central part of Figure 1a) that receive excitatory and inhibitory feedback from local interneurons and an excitatory input from neighboring cortical units and subcortical structures like the thalamus. Actually the excitatory feedback must be considered as coming from both local pyramidal neurons and genuine excitatory interneurons like spiny stellate cells.

2.1 Equations of the Model. Figure 1b is a translation of Figure 1a in the language of system theory. It represents the mathematical operations

performed inside such a cortical unit. The excitatory input is represented by an arbitrary average firing rate $p(t)$, which can be random (accounting for a nonspecific background activity) or deterministic, accounting for some specific activity in other cortical units. The three families—pyramidal neurons, excitatory interneurons, and inhibitory interneurons—and synaptic interactions between them are modeled by different systems.

The postsynaptic systems $P_i, i = 1, 2, 3$ (labeled $h_e(t)$ or $h_i(t)$ in the figure) convert the average firing rate describing the input to a population into an average excitatory (EPSP) or inhibitory (IPSP) postsynaptic potential. From the signal processing standpoint, they are linear stationary systems that are described by either a convolution with an impulse response function or, equivalently, a second-order linear differential equation. They have been proposed by van Rotterdam et al. (1982) in order to reproduce well the characteristics of real EPSPs and IPSPs. The impulse response function is of the form

$$h(t) = \begin{cases} \alpha\beta t e^{-\beta t} & t \geq 0 \\ 0 & t < 0 \end{cases}.$$

In other words, if $x(t)$ is the input to the system, its output $y(t)$ is the convolution product $h * x(t)$.

The constants α and β are different in the excitatory and inhibitory cases. α, expressed in millivolts, determines the maximal amplitude of the postsynaptic potentials; β, expressed in s^{-1}, lumps together characteristic delays of the synaptic transmission, that is, the time constant of the membrane and the different delays in the dendritic tree (Freeman, 1975; Jansen et al., 1993).

The corresponding differential equation is

$$\ddot{y}(t) = \alpha\beta x(t) - 2\beta\dot{y}(t) - \beta^2 y(t). \tag{2.1}$$

In the excitatory (resp. inhibitory) case, we have $\alpha = A$, $\beta = a$ (resp. $\alpha = B$, $\beta = b$). This second-order differential equation can be conveniently rewritten as a system of two first-order equations:

$$\begin{cases} \dot{y}(t) = z(t) \\ \dot{z}(t) = \alpha\beta x(t) - 2\alpha z(t) - \alpha^2 y(t) \end{cases}. \tag{2.2}$$

The sigmoid systems introduce a nonlinear component in the model. They are the gain functions that transform the average membrane potential of a neural population into an average firing rate (see, e.g., Gerstner & Kistler, 2002):

$$\mathrm{Sigm}(v) = \frac{\nu_{\max}}{2}\left(1 + \tanh\frac{r}{2}(v - v_0)\right) = \frac{\nu_{\max}}{1 + e^{r(v_0 - v)}},$$

where $\nu_{\max}$ is the maximum firing rate of the families of neurons, v_0 is the value of the potential for which a 50% firing rate is achieved, and r is the slope of the sigmoid at v_0; v_0 can be viewed as either a firing threshold or the excitability of the populations. This sigmoid transformation approximates the functions proposed by the neurophysiologist Walter Freeman (1975) to model the cell body action of a population.

The connectivity constants $C_1, \ldots, C_4$ account for the number of synapses established between two neuron's populations. We will see that they can be reduced to a single parameter C.

There are three main variables in the model—the outputs of the three postsynaptic boxes noted y_0, y_1, and y_2 (see Figure 1b). We also consider their derivatives $\dot{y}_0$, $\dot{y}_1$, $\dot{y}_2$, noted y_3, y_4, and y_5, respectively. If we write two equations similar to equation 2.2 for each postsynaptic system, we obtain a system of six first-order differential equations that describes Jansen's neural mass model:

$$\begin{cases} \dot{y}_0(t) = y_3(t) \; \dot{y}_3(t) = Aa\,\mathrm{Sigm}[y_1(t) - y_2(t)] - 2a\,y_3(t) - a^2 y_0(t) \\ \dot{y}_1(t) = y_4(t) \; \dot{y}_4(t) = Aa\{p(t) + C_2\,\mathrm{Sigm}[C_1\,y_0(t)]\} - 2a\,y_4(t) - a^2 y_1(t) \\ \dot{y}_2(t) = y_5(t) \; \dot{y}_5(t) = BbC_4\,\mathrm{Sigm}[C_3\,y_0(t)] - 2b\,y_5(t) - b^2 y_2(t). \end{cases} \quad (2.3)$$

We focus on the variable $y = y_1 - y_2$, the membrane potential of the main family of neurons (see Figure 1b). We think of this quantity as the output of the unit because in the cortex, the pyramidal cells are the main vectors of long-range cortico-cortical connections. Besides, their electrical activity corresponds to the EEG signal: pyramidal neurons throw their apical dendrites to the superficial layers of the cortex where the postsynaptic potentials are summed, accounting for the essential part of the EEG activity (Kandel, Schwartz, & Jessel, 2000).

2.2 Numerical Values of the Parameters. The parameters A, B, a, and b have been adjusted by van Rotterdam et al. (1982) to reproduce some basic properties of real postsynaptic potentials and make the system produce alpha activity. These authors set $A = 3.25$ mV, $B = 22$ mV, $a = 100\ \mathrm{s}^{-1}$, and $b = 50\ \mathrm{s}^{-1}$.

The excitability of cortical neurons can vary as a function of the action of several substances, and v_0 could potentially take different values, though we will use $v_0 = 6$ mV as suggested by Jansen on the basis of experimental studies due to Freeman (1987). The works of the latter also suggest that $\nu_{\max} = 5s^{-1}$ and $r = 0.56\ \mathrm{mV}^{-1}$, the values used by Jansen and Rit (1995).

The connectivity constants $C_i, i = 1, \ldots, 4$ are proportional to the average number of synapses between populations. On the basis of several neuroanatomical studies (Braitenberg and Schüz, 1998, among others) where these quantities had been estimated by counting synapses, Jansen and Rit

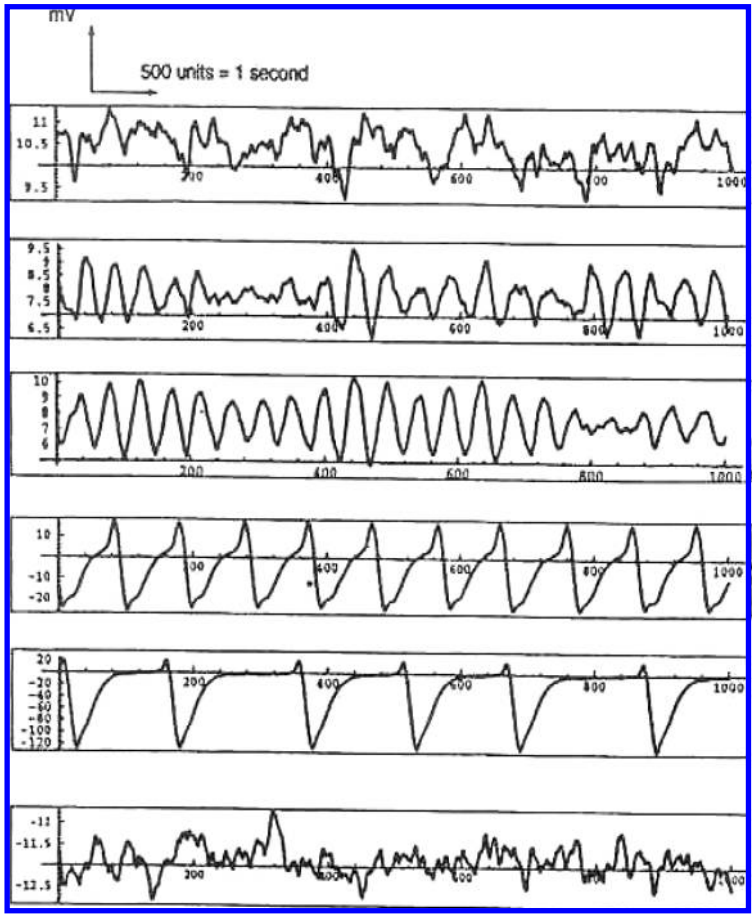

Figure 2: Activities of the unit shown in Figure 1 when simulated with a uniformly distributed white noise (between 120 and 320 Hz) as input. The different curves show different activities depending on the value of the parameter C. The third curve from the top looks like alpha activity and has been obtained for $C = 135$ (from Jansen & Rit, 1995).

succeeded in reducing them to fractions of a single parameter C:

$$\begin{cases} C_1 = C & C_2 = 0.8C \\ C_3 = 0.25C & C_4 = 0.25C \end{cases}.$$

Jansen and Rit varied C to observe alpha-like activity and obtained it for $C = 135$ (see Figure 2).

In summary, previous work shows that the following set of parameters allows the neural mass model described by equations 2.3 to produce a set of EEG-like signals:

$$\begin{cases} A = 3.25 & B = 22 \\ a = 100 & b = 50 \\ v_0 = 6 & C = 135 \end{cases}. \tag{2.4}$$

We show in section 3.4 that the behavior of the neural mass model is fairly sensitive to the choice of the values of these parameters. Indeed, changes as small as 5% in these values produce some fairly different behaviors.

The quantity p represents the lumped activity of the brain areas connected to the unit. Jansen and Rit (1995) chose $p(t)$ to be a uniformly distributed noise ranging from 120 to 320 pulses per second, as they wanted to model nonspecific input (they used the term *background spontaneous activity*). This noise dynamics allowed them to produce alpha-like activity. Similarly, Wendling and his colleagues (2000) used a white gaussian noise (mean 90 and standard deviation 30) for $p(t)$ and observed the emission of spikes that was reminiscent of an epileptic activity. We show in the next section that these two different behaviors can be nicely accounted for by a geometric study of system 2.3 through its bifurcations.

3 Bifurcations and Oscillations

In this section we consider p as a parameter of the system and propose to study the behavior of a unit when p varies. We therefore study the dynamical system 2.3, with all parameters but p being kept constant and equal to the values set by Jansen and Rit (1995) (see equation 2.4). In section 3.4 we extend this analysis to other values of the parameters in equation 2.4. Let $Y = (y_0, \ldots, y_5)^T$; the system has the form

$$\dot{Y} = f(Y, p),$$

where f is the smooth map from $\mathbb{R}^6$ to $\mathbb{R}^6$ given by equation 2.3 and p is a parameter.

We are interested in computing the fixed points and periodic orbits of the system as functions of p because they will allow us to account for the appearance of such activities as those shown in Figure 2 (alpha-like activity) and Figure 3 (epileptic spike-like activity).

3.1 Fixed Points

3.1.1 The One Parameter Family of Fixed Points. We look for the points Y where the vector field $f(., p)$ vanishes (called *fixed points*, *critical points*, or

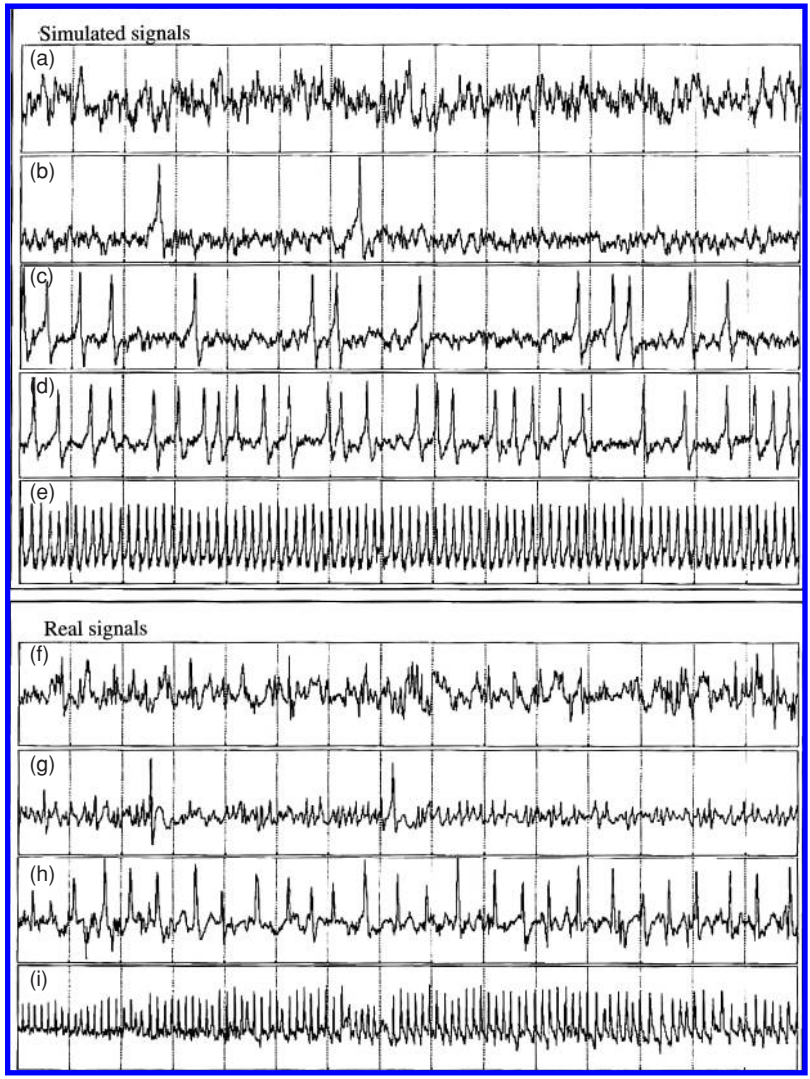

Figure 3: (a–e) Activities of the unit shown in Figure 1 when simulated with a white gaussian noise as input (corresponding to an average firing rate between 30 and 150 Hz). The authors varied the excitation/inhibition ratio A/B. As this ratio is increased, we observe sporadic spikes followed by increasingly periodic activities. (f–i) Real activities recorded from epileptic patients before (f,g) and during a seizure (h,i). (From Wendling et al. 2000.)

equilibrium points). Writing $\dot{Y} = 0$, we obtain the system of equations

$$\begin{cases} y_0 = \frac{A}{a}\text{Sigm}[y_1 - y_2] & y_3 = 0 \\ y_1 = \frac{A}{a}(p + C_2\text{Sigm}[C_1 y_0]) & y_4 = 0 \\ y_2 = \frac{B}{b}C_4\text{Sigm}[C_3 y_0] & y_5 = 0, \end{cases} \tag{3.1}$$

which leads to the (implicit) equation of the one-parameter family of equilibrium points in the $(p, y = y_1 - y_2)$ plane:

$$y = \frac{A}{a}p + \frac{A}{a}C_2\text{Sigm}\left[\frac{A}{a}C_1\text{Sigm}(y)\right] - \frac{B}{b}C_4\text{Sigm}\left[\frac{A}{a}C_3\text{Sigm}(y)\right]. \tag{3.2}$$

As mentioned before, $y = y_1 - y_2$ can be thought of as representing the EEG activity of the unit, and p is our parameter of interest. We show the curve defined by equation 3.2 in Figure 4a. The number of intersections between this curve and a vertical line of equation $p = constant$ is the number of equilibrium points for this particular value of p. We notice that for $p \approx 110$–120, the system goes from three equilibrium points to a single one. We also note that the curve has been drawn for some negative values of p. These points do not have any biological meaning since p is a firing rate. It turns out, though, that they play a central role in the mathematical description of the model (see section 3.2).

The coordinates of the singular points cannot be written explicitly as functions of p, but every singular point is completely determined by the quantity y. More precisely, the coordinates of every singular point $S(y)$ have the following form:

$$S(y) = \left(\frac{A}{a}\text{Sigm}(y) \quad \frac{A}{a}\left(p + C_2\text{Sigm}\left[C_1\frac{A}{a}\text{Sigm}(y)\right]\right) \right.$$
$$\left. \frac{B}{b}C_4\text{Sigm}\left[C_3\frac{A}{a}\text{Sigm}(y)\right] \quad 0 \quad 0 \quad 0\right)^{\top}, \tag{3.3}$$

p and y being related through equation 3.2.

3.1.2 Local Study Near the Singular Points. In order to study the behavior of the system near the fixed points, we linearize it and calculate its Jacobian matrix, that is, the partial derivative $\mathcal{J}$ of $f(., p)$ at the fixed point $S(y)$. It is easy but tedious to show that at the fixed point $S(y)$, we have

$$\mathcal{J}(S(y)) = \begin{pmatrix} 0_3 & I_3 \\ KM(y) & -K \end{pmatrix},$$

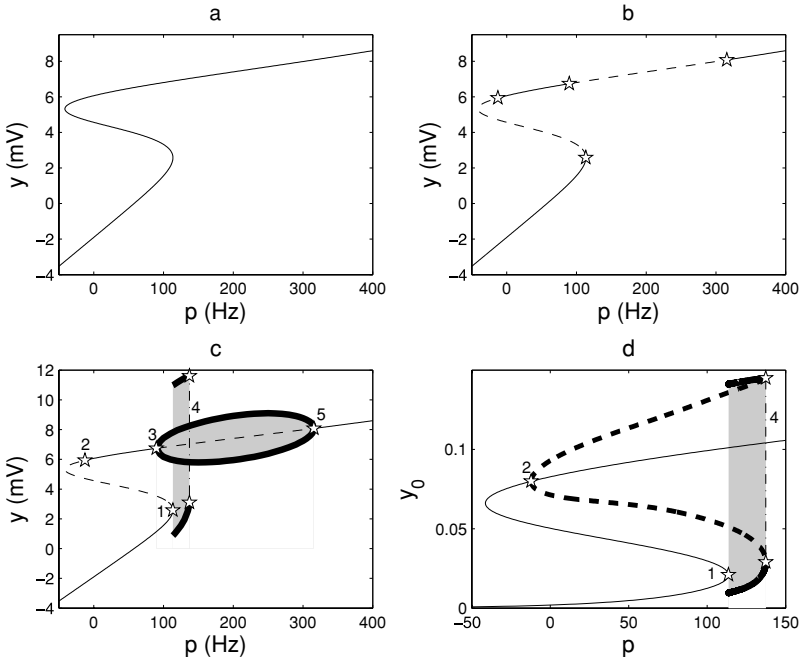

Figure 4: (a) Curve defined by equation 3.2. For each value of p, the curve yields the coordinate(s) y of the corresponding fixed point(s). (b) Fixed points and their stability. Stable fixed points lie on the solid portions of the curve, and unstable points lie on the dashed ones. Stars correspond to transition points where the Jacobian matrix has some eigenvalues with zero real part. (c) Curve of the fixed points with two branches of limit cycles (shaded regions bounded by thick black curves). The stars labeled 3 and 5 are Hopf bifurcation points. The oval between them is the branch of Hopf cycles: for each $89.83 \leq p \leq 315.70$, the thick black curves between points 3 and 5 give the highest and lowest y values attained by the Hopf cycle. The other branch of limit cycles lies in the domain between the star labeled 1, where there is a saddle node bifurcation with homoclinic orbit, and the dash-dotted line 4 representing a fold bifurcation of limit cycles. This kind of representation is called a bifurcation diagram. (d) A Hopf bifurcation at the point labeled 2 ($p = -12.15$) gives rise to a branch of unstable limit cycles that merges with the branch of stable cycles lying between the point labeled 1 and the dashed line labeled 4. This phenomenon is called a fold bifurcation of limit cycles.

where

$$K = 2\mathrm{diag}(a, a, b),\ M(y) = \begin{pmatrix} -a/2 & \gamma(y) & -\gamma(y) \\ \delta(y) & -a/2 & 0 \\ \theta(y) & 0 & -b/2 \end{pmatrix},$$

I_3 is the three-dimensional identity matrix, and 0_3 is the three-dimensional null matrix. The three functions γ, δ, and θ are defined by

$$\gamma(y) = \frac{A}{2}\mathrm{Sigm}'(y)$$
$$\delta(y) = \frac{AC_1C_2}{2}\mathrm{Sigm}'(C_1 y_0(y))$$
$$\theta(y) = \frac{BC_3C_4}{2}\mathrm{Sigm}'(C_3 y_0(y)),$$

where $y_0(y)$ is the first coordinate of $S(y)$ and Sigm′ is the derivative of the function Sigm.

We compute the eigenvalues of $\mathcal{J}$ along the curve of Figure 4a to analyze the stability of the family of equilibrium points. The results are summarized in Figure 4b. The solid portions of curve correspond to stable fixed points (all eigenvalues have a negative real part) and the dashed ones to unstable fixed points (some eigenvalues have a positive real part). Stars indicate points where at least one eigenvalue of the system crosses the imaginary axis, therefore having a zero real part. These points are precious landmarks for the study of bifurcations of the system.

3.2 Bifurcations and Oscillatory Behavior in Jansen's Model. A bifurcation is a drastic and sudden change in the behavior of a dynamic system that occurs when one or several of its parameters are varied. Often it corresponds to the appearance or disappearance of limit cycles. Describing oscillatory behaviors in Jansen's model is therefore closely related to studying its bifurcations. In our case, when p varies from $-\infty$ to $+\infty$, the system undergoes five bifurcations (remember that only the positive values of p are biologically relevant).

We now describe these bifurcations from a somewhat intuitive viewpoint, but our results are grounded in the mathematical theory of bifurcations (Perko, 2001; Ioos & Adelmeyer, 1999; Kuznetsov, 1998; Berglund, 2001a, 2001b) and the extensive use of the software *XPP-Aut* due to Bard Ermentrout (available on http://www.pitt.edu/∼phase/). We were also inspired by bifurcation studies of single-neuron models (see Izhikevich, in press; Hoppenstaedt & Izhikevich, 1997; Rinzel & Ermentrout, 1998).

3.2.1 Hopf Bifurcations and Alpha Activity in Jansen's Model. When p is varied smoothly, the eigenvalues of the fixed points move smoothly in the complex plane: when two complex conjugate eigenvalues cross the imaginary axis, the system undergoes in general what is called a *Hopf bifurcation*. Two of them happen in Jansen's model (if we ignore the negative values of p) for $p = 89.83$ and $p = 315.70$. A theorem due to Hopf (Perko, 2001)

shows[1] that for $p = 89.83$, a one-parameter family of stable periodic orbits appears at the fixed point that has two complex conjugate eigenvalues crossing the imaginary axis toward positive real parts. These periodic orbits persist until $p = 315.70$, where a second Hopf bifurcation occurs: the two eigenvalues whose real parts became positive for $p = 89.83$ see them become negative again, corresponding to the (re)creation of a simple, attractive fixed point. This is shown in Figure 4c: for p between 89.83 and 315.70, there is a family of periodic orbits (we call them *Hopf cycles* from now on) parameterized by p for which the minimal and maximal y values have been plotted (thick oval curve). Numerically, using XPP-Aut, we find that these oscillations have a frequency around 10 Hz, which corresponds to alpha activity. So it appears that alpha-like activity in Jansen's model is determined by Hopf cycles. Interestingly enough, the system does not display any Hopf bifurcation if we approximate the sigmoid by a piecewise linear function, or if we try to reduce the dimensionality of the system by singular perturbation theory (Berglund 2001b). In both cases, the system is unable to produce alpha activity.

Let us interpret Jansen and Rit's results in the light of our mathematical analysis. They report observing alpha activity (see the third curve in Figure 2) when they use a uniformly distributed noise in the range 120 to 320 Hz at the entry of the system. This is easy to account for if we look at Figure 4c: in this domain of p values, the Hopf cycles are essentially the only attractors of the dynamical system 2.3. So at every time instant t, its trajectories will tend to coil around the Hopf cycle corresponding to $p = p(t)$. We will therefore see oscillations of constant frequency and varying amplitude leading to the waxing and waning activity reported by Jansen and Rit.

3.2.2 Global Bifurcations and Spike-Like Epileptic Activity. Hopf bifurcations are called local because their appearance depends on only local properties of the dynamical system around the bifurcation point. In Figure 3, we see that the system is able to display spike-like activities that resemble certain epileptic EEG recordings (Wendling et al., 2000). These activities arise from a branch of large stable periodic orbits delimited by a pair of global bifurcations (i.e., depending not only on local properties of the dynamical system) that correspond to the star labeled 1 and the dash-dotted line labeled 4 in Figure 4c. From now on, we will call these orbits *spike cycles*.

The branch of spike cycles begins for $p = 113.58$, thanks to a saddle-node bifurcation with homoclinic orbit[2] (see Perko, 2001; Kuznetsov, 1998). It ends for $p = 137.38$ because of a fold bifurcation of limit cycles that we

[1] The proof of the existence of a Hopf bifurcation relies on the calculation of the Lyapunov number at the bifurcation points. It is quite technical and is not developed here.

[2] The proof of the existence of this saddle node bifurcation with homoclinic orbit uses a theorem due to Shil'nikov (Kuznetsov, 1998).

identified with XPP-Aut. This bifurcation results from the fusion of a stable and an unstable family of periodic orbits. The stable family is the branch of spike cycles, and the unstable family originates from a Hopf bifurcation occuring at $p = -12.15$.

Thanks to XPP-Aut, we have been able to plot the folding and the associated Hopf bifurcation with respect to the y_0 axis (see Figure 4d). So far we have shown the bifurcation diagrams in the (p, y) plane, but for technical reasons due to XPP-Aut, we show the bifurcation diagram in the (p, y_0) plane in this case. Its general properties are the same, though. For example, we recognize the S shape of the fixed points diagram and the relative position of landmarks 1, 2, and 4.

Contrary to the Hopf cycles whose periods remains around 10 Hz, the spike cycles can display every frequency in the range 0 to 5 Hz (it increases with p) so that they are able to reproduce the various "spiking" activities observed in Figure 3.

In this case also we can identify the central role played by p in shaping the output of the unit. Wendling et al. (2000) used a gaussian noise with mean 90 and standard deviation 30 to produce the spikes in Figure 3, resulting in an input to the unit essentially varying between 30 and 150 Hz, which is quite low compared to the range used by Jansen and Rit (1995). Let us first distinguish two parts in the curve of fixed points in Figure 4c. We call the set of stable fixed points below the star labeled 1 *lower branch* and the one between the stars labeled 2 and 3 *upper branch*. For p between 30 and 90, the system displays a classical bistable behavior with two stable fixed points (one on each branch), the lowest fixed points appearing to be dominant. We found experimentally that the basin of attraction of the upper point is not very large, so that one has to start quite close to it in order to converge to it. As a result, a low input ($p \leq 90$) produces in general a low output: the trajectory is attracted by the lower branch. For p between 110 and 140, we are in the range of p values where spike-like activity can appear and spiking competes with Hopf cycles, but trajectories near the lower branch are attracted by spike cycles (as we will see in section 3.3), hence producing spike-shaped activities. These two facts—attraction to the lower branch and preference of the lower branch for spike cycles—allow us to understand how the model can produce epileptic-like activities.

3.3 Synthesis: Behavior of the Cortical Unit Model According to the Input Parameter p. We now have in hand all the ingredients to describe the activity of this neural mass model when stimulated by a slowly varying input. For that purpose, we computed two trajectories (or orbits) of the system with p increasing linearly in time at a slow rate ($\mathrm{d}p/\mathrm{d}t = 1$). The system was initialized at the two stable fixed points at $p = 0$: the stable state on the lower branch and the one on the upper branch (see the stars in Figure 5). As long as $p \leq 89.83$, the two trajectories are flat, following their respective branches of fixed points (see Figure 6, $p = 80$). After the Hopf

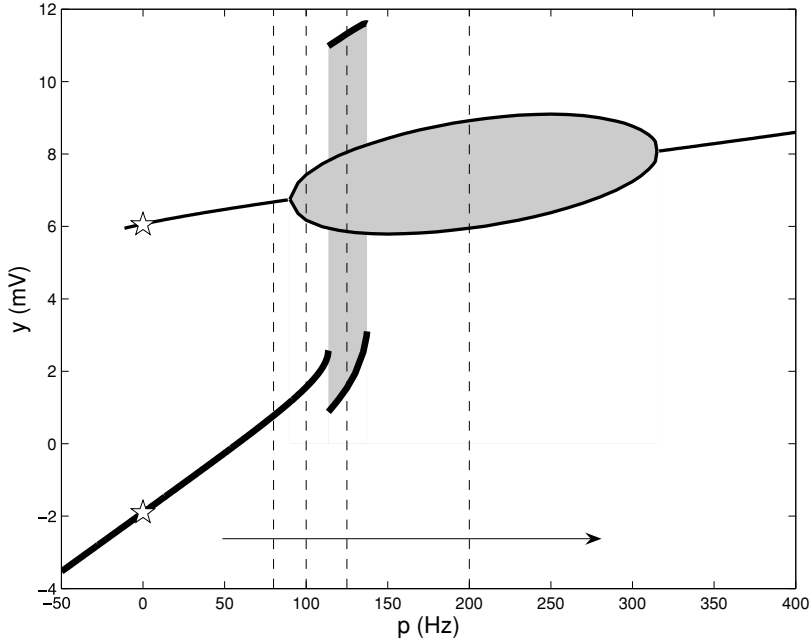

Figure 5: Diagram of the stable attractors (stable fixed points and stable limit cycles) of the model described by equations 2.3. The stars show the starting points of the two trajectories we simulated with p slowly increasing. Their time courses have been frozen for $p = 80$, 100, 125, and 200 (as indicated by the vertical dashed lines on this figure) and can be seen in Figure 6. Lower and upper states of the unit correspond to the thick and thin lines, respectively.

bifurcation occurring at $p = 89.83$, the orbit corresponding to the upper branch naturally coils on the Hopf cycles branch (see Figure 6, $p = 100$), resulting in alpha-like activity. The trajectory on the lower branch does the same with the spike cycles as soon as p reaches the value 113.58 (see Figure 6, $p = 125$). As $p \geq 137.38$, the only remaining attractor is the Hopf cycle branch so that the system can exhibit only alpha-like behavior (see Figure 6, $p = 200$). For high values of p ($\geq$315.70), there is only one stable fixed point, and the trajectory is flat again. These results lead us to distinguish two states, the lower and the upper, for the unit. The lower state is described by the combination of the lower branch of fixed points that correspond to rest and the spike cycles (thick lines in Figure 5). It corresponds to positive values of p less than 137.38. The upper state is described by the upper branch of fixed points, the Hopf cycle branch, and the branch of fixed points following it (thin lines in Figure 5). It corresponds to positive values of p. These states are relevant for slow dynamics of the input p. In effect, a trajectory starting

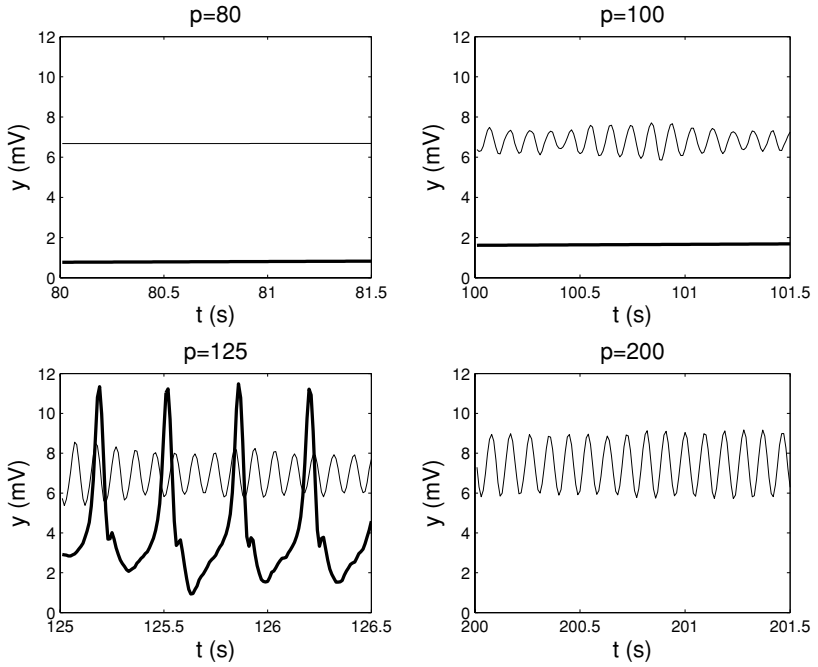

Figure 6: Activities produced by Jansen's neural mass model for typical values of the input parameter p (see the text). The thin (resp. thick) curves are the time courses of the output y of the unit in its upper (resp. lower) state. For $p > 137.38$, there is only one possible behavior of the system. In the case of oscillatory activities, we added a very small amount of noise to p (a zero mean gaussian noise with standard deviation 0.05).

near one of these states will stay in its neighborhood when p is varied slowly (increasing or decreasing). When the unit is in its lower-state and p becomes larger than 137.38, it jumps to its upper state and cannot return to its lower state (if p varies slowly). Therefore, when in its upper state, a unit essentially produces alpha-like activity, and its input must be decreased abruptly to bring it back to its lower state. Conversely, starting in the lower state, a unit can be brought to the upper state by an abrupt increase of its input. It can also stay in its lower state regime, between rest and spiking, if the input and its variation remain moderate.

3.4 What About Other Parameters? We think that the bifurcation analysis with respect to p is the most relevant since this parameter is expected to vary more and faster than the others, but it is interesting to build bifurcation diagrams with respect to p with different settings of the other parameters.

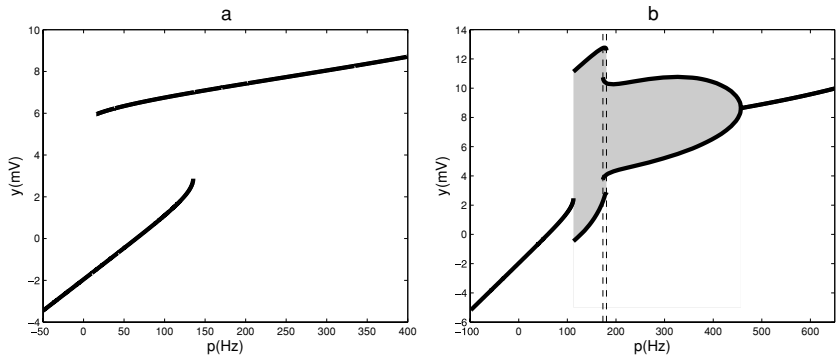

Figure 7: The stable attractors of the system in two typical cases encountered for different settings of parameters A, B, C, a, or b. (a) Corresponds to lower (resp. higher) values of A, B, C (resp. a and b) than those given by equation 2.4. Here, $A = 3$ instead of 3.25: there are no more limit cycles. (b) Corresponds to higher (resp. lower) values of A, B, C (resp. a and b). Here $C = 140$ instead of 135. The spiking behavior is more prominent and is the only one available in a wide range of p values ($112.6 \leq p \leq 173.1$). Except in a narrow band ($173.1 \leq p \leq 180.4$), the system displays one single behavior for each value of p.

We indeed observed that varying any parameter by more than 5% leads to quite drastic changes in the bifurcation diagram and to significantly less rich behaviors of the unit. These changes fall into two broad categories (see Figure 7).

For low values of A, B, or C or high values of a or b, the system is no longer able to produce oscillations (see Figure 7a). For high values of A, B, or C or low values of a or b, we observed a new kind of bifurcation diagram (an example is given in Figure 7b). In this regime, the system has only one stable state for each value of p, except sometimes in a narrow range of p values (in the figure, $173.1 \leq p \leq 180.4$). The range where spiking can occur is broader and the one for alpha activity is severely truncated. Moreover, spiking does not coexist with alpha rhythm anymore so that (except for a very small range of p values) it is the only available behavior on a broad interval of p values (in the figure, $112.6 \leq p \leq 173.1$). So spiking becomes really prominent.

The mathematical explanation for this new diagram is the fusion of the Hopf cycles branch with the branch of unstable periodic orbits that can be seen in Figure 4d. It results in a new organization of periodic orbit branches. We have two stable branches (for $112.6 \leq p \leq 180.4$ and $173.1 \leq p \leq 457.1$), linked by a branch of unstable orbits. Transitions between stable and unstable orbits are made via fold bifurcations of limit cycles like the one in Figure 4d.

4 Conclusion

The bifurcation diagram (see Figure 5) is a precious tool to describe Jansen's neural mass model's behaviors for constant or slowly varying stimulus. We also showed that this analysis provided a good basis for understanding what happened when the input was noisy. In the case of small or slow variations of this input, the model can be reduced to a binary unit with two possible states.

When we studied how the bifurcation diagram varied when changing the values of the other model's parameters, it appeared that Jansen's model's behavior was quite sensitive to the choice of the physiological parameters A, B, C, a, and b. Variations of a few percentages in the values of these parameters can cause drastic changes in the qualitative behavior of this neural mass model. Detailed comparisons of these behaviors with experimental data should be essential for further validation of the model and for defining ways to make it evolve.

What about the behavior of spatial assemblies of such models? Jansen et al. have studied evoked potentials in two connected cortical units (Jansen & Rit, 1995; Jansen et al., 1993) and Wendling et al. (2000) have simulated an epileptogenic network composed of three units. There are still no studies involving an arbitrary number of such units or a continuum of them.

This is a difficult task for at least three reasons. First, the size of the system of differential equations describing the network increases linearly with the number of units, making its mathematical analysis even more difficult. Second, the nonlinearities in the model and the network open the door to emerging properties impossible to predict from the sole knowledge of the behavior of one unit. Third, the way to connect those units is an open question since our knowledge of anatomical connectivity in the cortex is still very poor. Nevertheless, we think this is an important area for future work.

Acknowledgments

This work was partially supported by Elekta Instrument AB.

References

Berglund, N. (2001a). *Geometrical theory of dynamical systems.* Citebase.

Berglund, N. (2001b). *Perturbation theory of dynamical systems.* Citebase.

Braitenberg, V., & Schüz, A. (1998). *Cortex: Statistics and geometry of neuronal connectivity* (2nd ed.). Berlin: Springer.

David, O., Cosmelli, D., & Friston, K. J. (2004). Evaluation of different measures of functional connectivity using a neural mass model. *Neurolmage, 21*, 659–673.

David, O., & Friston, K. J. (2003). A neural mass model for MEG/EEG: Coupling and neuronal dynamics. *Neurolmage, 20*, 1743–1755.

Freeman, W. (1975). *Mass action in the nervous system.* New York: Academic Press.
Freeman, W. (1987). Simulation of chaotic EEG patterns with a dynamic model of the olfactory system. *Biological Cybernetics, 56*, 139–150.
Gerstner, W., & Kistler, W. M. (2002). Mathematical formulations of Hebbian learning. *Biol. Cybern., 87*, 404–415.
Hoppenstaedt, F., & Izhikevich, E. (1997). *Weakly connected neural networks.* New York: Springer-Verlag.
Ioos, G., & Adelmeyer, M. (1999). *Topics in bifurcation theory and applications* (2nd ed.). Singapore: World Scientific.
Izhikevich, E. M. (in press). *Dynamical systems in neuroscience: The geometry of excitability and bursting.* Cambridge, MA: MIT Press.
Jansen, B. H., & Rit, V. G. (1995). Electroencephalogram and visual evoked potential generation in a mathematical model of coupled cortical columns. *Biol. Cybern., 73*, 357–366.
Jansen, B. H., Zouridakis, G., & Brandt, M. E. (1993). A neurophysiologically-based mathematical model of flash visual evoked potentials. *Biological Cybernetics, 68*, 275–283.
Kandel, E., Schwartz, J., & Jessel, T. (2000). *Principles of neural science* (4th ed.). New York: McGraw-Hill.
Kuznetsov, Y. A. (1998). *Elements of applied bifurcation theory.* (2nd ed.). New York: Springer.
Lopes da Silva, F., Hoeks, A., & Zetterberg, L. (1974). Model of brain rhythmic activity. *Kybernetik, 15*, 27–37.
Lopes da Silva, F., van Rotterdam, A., Barts, P., van Heusden, E., & Burr, W. (1976). Model of neuronal populations: The basic mechanism of rhythmicity. In M. A. Corner & D. F. Swaab (Eds.), *Progress in brain research* (pp. 281–308). Amsterdarm: Elsevier.
Perko, L. (2001). *Differential equations and dynamical systems* (3rd ed.). New York: Springer.
Rinzel, J., & Ermentrout, G. (1998). Analysis of neuronal excitability and oscillations. In C. Koch & I. Segev (Eds.), *Methods in neuronal modeling: From ions to networks* (pp. 251–291). Cambridge, MA: MIT Press.
van Rotterdam, A., Lopes da Silva, F., van den Ende, J., Viergever, M., & Hermans, A. (1982). A model of the spatial-temporal characteristics of the alpha rhythm. *Bulletin of Mathematical Biology, 44*(2), 283–305.
Wendling, E, Bellanger, J., Bartolomei, F., & Chauvel, P. (2000). Relevance of nonlinear lumped-parameter models in the analysis of depth-EEG epileptic signals. *Biological Cybernetics, 83*, 367–378.

Received September 23, 2005; accepted April 28, 2006.

This article has been cited by:

1. Basabdatta Sen Bhattacharya, Yuksel Cakir, Neslihan Serap-Sengor, Liam Maguire, Damien Coyle. 2012. Model-based bifurcation and power spectral analyses of thalamocortical alpha rhythm slowing in alzheimer's disease. *Neurocomputing* . [CrossRef]
2. B. Seymour. 2012. Hodgkin and Huxley's legacy: the science of neural supercomputing. *Brain* **135**:9, 2892-2895. [CrossRef]
3. Alex Blenkinsop, Antonio Valentin, Mark P. Richardson, John R. Terry. 2012. The dynamic evolution of focal-onset epilepsies - combining theoretical and clinical observations. *European Journal of Neuroscience* **36**:2, 2188-2200. [CrossRef]
4. Marc Goodfellow, Kaspar Schindler, Gerold Baier. 2012. Self-organised transients in a neural mass model of epileptogenic tissue dynamics. *NeuroImage* **59**:3, 2644-2660. [CrossRef]
5. Alejo J. Nevado-Holgado, Frank Marten, Mark P. Richardson, John R. Terry. 2012. Characterising the dynamics of EEG waveforms as the path through parameter space of a neural mass model: Application to epilepsy seizure evolution. *NeuroImage* **59**:3, 2374-2392. [CrossRef]
6. Oscar Benjamin, Thomas H.B. Fitzgerald, Peter Ashwin, Krasimira Tsaneva-Atanasova, Fahmida Chowdhury, Mark P Richardson, John R Terry. 2012. A phenomenological model of seizure initiation suggests network structure may explain seizure frequency in idiopathic generalised epilepsy. *The Journal of Mathematical Neuroscience* **2**:1, 1. [CrossRef]
7. Jonathan Touboul, Fabrice Wendling, Patrick Chauvel, Olivier Faugeras. 2011. Neural Mass Activity, Bifurcations, and Epilepsy. *Neural Computation* **23**:12, 3232-3286. [Abstract] [Full Text] [PDF] [PDF Plus]
8. Roberto C. Sotero, Amir Shmuel. 2011. Energy-based stochastic control of neural mass models suggests time-varying effective connectivity in the resting state. *Journal of Computational Neuroscience* . [CrossRef]
9. R. Hindriks, F. Bijma, B.W. van Dijk, Y.D. van der Werf, E.J.W. van Someren, A.W. van der Vaart. 2011. Dynamics underlying spontaneous human alpha oscillations: A data-driven approach. *NeuroImage* **57**:2, 440-451. [CrossRef]
10. Marc Goodfellow, Kaspar Schindler, Gerold Baier. 2011. Intermittent spike–wave dynamics in a heterogeneous, spatially extended neural mass model. *NeuroImage* **55**:3, 920-932. [CrossRef]
11. A.J. Pons, Jose L. Cantero, Mercedes Atienza, Jordi Garcia-Ojalvo. 2010. Relating structural and functional anomalous connectivity in the aging brain via neural mass modeling. *NeuroImage* **52**:3, 848-861. [CrossRef]
12. S. Coombes. 2010. Large-scale neural dynamics: Simple and complex. *NeuroImage* **52**:3, 731-739. [CrossRef]

13. Andreas Spiegler, Stefan J. Kiebel, Fatihcan M. Atay, Thomas R. Knösche. 2010. Bifurcation analysis of neural mass models: Impact of extrinsic inputs and dendritic time constants. *NeuroImage* **52**:3, 1041-1058. [CrossRef]

14. Mauro Ursino, Filippo Cona, Melissa Zavaglia. 2010. The generation of rhythms within a cortical region: Analysis of a neural mass model. *NeuroImage* **52**:3, 1080-1094. [CrossRef]

15. Pedro A. Valdés-Hernández, Alejandro Ojeda-González, Eduardo Martínez-Montes, Agustín Lage-Castellanos, Trinidad Virués-Alba, Lourdes Valdés-Urrutia, Pedro A. Valdes-Sosa. 2010. White matter architecture rather than cortical surface area correlates with the EEG alpha rhythm. *NeuroImage* **49**:3, 2328-2339. [CrossRef]

16. W.D. Penny, V. Litvak, L. Fuentemilla, E. Duzel, K. Friston. 2009. Dynamic Causal Models for phase coupling. *Journal of Neuroscience Methods* **183**:1, 19-30. [CrossRef]

17. Niranjan Chakravarthy, Kostas Tsakalis, Shivkumar Sabesan, Leon Iasemidis. 2009. Homeostasis of Brain Dynamics in Epilepsy: A Feedback Control Systems Perspective of Seizures. *Annals of Biomedical Engineering* **37**:3, 565-585. [CrossRef]

18. Olivier Faugeras, Romain Veltz, François Grimbert. 2009. Persistent Neural States: Stationary Localized Activity Patterns in Nonlinear Continuous n-Population, q-Dimensional Neural Networks. *Neural Computation* **21**:1, 147-187. [Abstract] [Full Text] [PDF] [PDF Plus]

19. Niranjan Chakravarthy, Shivkumar Sabesan, Kostas Tsakalis, Leon Iasemidis. 2009. Controlling epileptic seizures in a neural mass model. *Journal of Combinatorial Optimization* **17**:1, 98-116. [CrossRef]

20. Stefan J. Kiebel, Marta I. Garrido, Rosalyn J. Moran, Karl J. Friston. 2008. Dynamic causal modelling for EEG and MEG. *Cognitive Neurodynamics* **2**:2, 121-136. [CrossRef]

21. Olivier Faugeras, François Grimbert, Jean-Jacques Slotine. 2008. Absolute Stability and Complete Synchronization in a Class of Neural Fields Models. *SIAM Journal on Applied Mathematics* **69**:1, 205-250. [CrossRef]